RESEARCH ARTICLE | AUGUST 14 2024

Magneto-optical Kerr effect of noncollinear antiferromagnetic Mn_3Ir films

Kihiro T. Yamada ; Kotarou Yamaguchi ; Yuta Kobayashi ; Yota Takamura ; Hiro Munekata ; Teruo Ono ; Takahiro Moriyama ; Takuya Satoh

AIP Advances 14, 085020 (2024)
https://doi.org/10.1063/5.0217261
CHORUS

AIP Advances ARTICLE pubs.aip.org/aip/adv

Magneto-optical Kerr effect of noncollinear antiferromagnetic Mn_3Ir films

Cite as: AIP Advances 14, 085020 (2024); doi: 10.1063/5.0217261
Submitted: 3 May 2024 • Accepted: 29 July 2024 •
Published Online: 14 August 2024

View Online Export Citation CrossMark

Kihiro T. Yamada,[1,a)] Kotarou Yamaguchi,[1] Yuta Kobayashi,[2] Yota Takamura,[3] Hiro Munekata,[1] Teruo Ono,[2,4] Takahiro Moriyama,[5,6] and Takuya Satoh[1]

AFFILIATIONS

[1] Department of Physics, Tokyo Institute of Technology, Tokyo 152-8551, Japan
[2] Institute for Chemical Research, Kyoto University, Uji, Kyoto 611-0011, Japan
[3] School of Engineering, Tokyo Institute of Technology, Tokyo 152-8550, Japan
[4] Center for Spintronics Research Network, Institute for Chemical Research, Kyoto University, Uji, Kyoto 611-0011, Japan
[5] Department of Materials Physics, Nagoya University, Furo-cho, Chikusa-ku, Nagoya 464-8603, Japan
[6] PRESTO, Japan Science and Technology Agency, Kawaguchi, Saitama 322-0012, Japan

[a)] **Author to whom correspondence should be addressed:** yamada@phys.titech.ac.jp

ABSTRACT

We present the magneto-optical Kerr effect (MOKE) of (111)-oriented antiferromagnetic $L1_2$-Mn_3Ir films epitaxially grown on MgO (111) substrates. We observed that the amplitude and sign of the polar MOKE change depending on the growth temperature. The Mn_3Ir films grown at 800 and 600 °C have rotation angles of 41.6 and −4.6 mdeg and ellipticity angles of −15.3 and 9.1 mdeg, respectively. Residual strains owing to heteroepitaxial growth on the order of a few tenths of a percent can play a critical role in determining the amplitude and sign of the MOKE of a noncollinear antiferromagnet, unlike ferromagnets.

Magneto-optical effects,[1] which change the polarization state of light interacting with magnetic materials, are now widely used to study magnetic domain structures[2,3] and the magnetism of novel materials.[4–7] The effect of reflection from a magnetic material on light polarization is called the magneto-optical Kerr effect (MOKE). MOKE generally appears in ferromagnetic and ferrimagnetic materials with abundant magnetization but not in antiferromagnets with no net magnetization. However, the MOKE of Kagome-type noncollinear antiferromagnets, such as Mn_3Sn,[7] manifests itself through the spin orbit coupling (SOC)[8,9] induced by the noncollinear spin configuration, which forms cluster octupole moments.[10] It should be noted that the cluster octupole moments[10] have the same symmetry as the magnetic dipole moments of ferromagnets. Following the discovery of the anomalous Hall effect, that is, MOKE in the DC limit, in Mn_3X systems,[11–17] MOKE in the visible spectral range was demonstrated in a Mn_3Sn single crystal first by Higo *et al.*[7] Inspired by this demonstration, several research groups reported MOKE in Mn_3Sn and Mn_3Ge systems.[18–21] The MOKE of Mn_3X systems originates from the non-vanishing Berry curvature caused by the combination of the noncollinear spin texture and SOC.[8,9,22–24] Therefore, because the atomistic SOC constant of Ir (546 meV) is greater than those of Sn (287 meV) and Ge (109 meV),[25] MOKE larger than those in Mn_3Sn and Mn_3Ge can be expected in Mn_3Ir.

In this study, we quantitatively investigated the polar MOKE of (111)-oriented $L1_2$-Mn_3Ir films with a noncollinear spin configuration and large SOC[25] [Fig. 1(a)]. The formation of the $L1_2$ order in Mn_3Ir is required for the large anomalous Hall effect.[8,15–17] Figure 1(b) shows the unit cell of $L1_2$-Mn_3Ir (space group $Pm\bar{3}m$). The Mn atoms on the (111) plane form a Kagome lattice. Mn spins form all-in/all-out spin textures owing to magnetic frustration caused by the influence of inter-site exchange interactions.[26] The Mn spin moments are slightly canted, generating a tiny net spin magnetization of 0.027 μ_B along the [111] direction.[24] $L1_2$-Mn_3Ir had two energetically degenerated spin configurations, A and B, as shown in Fig. 1(b). Because the Berry curvature is finite along the [111] axis, which is a common axis of the three mirror planes

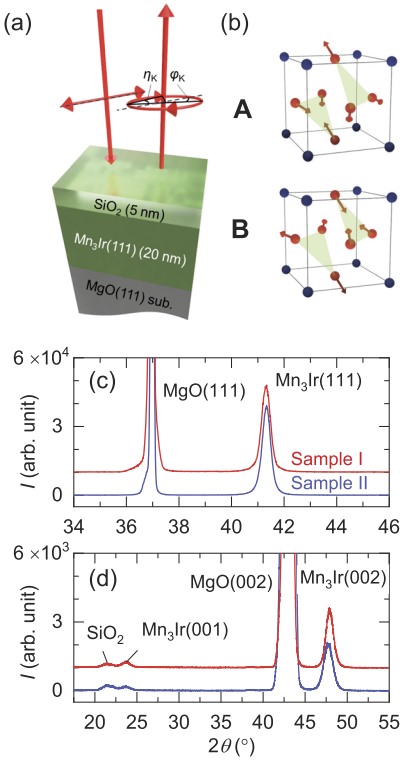

FIG. 1. (a) Experimental geometry for measuring the polar magneto-optical Kerr effect (MOKE) of (111)-oriented Mn_3Ir film. (b) Unit cell and spin configurations of $L1_2$-Mn_3Ir. (c) Out-of-plane θ–2θ X-ray diffraction (XRD) patterns. (d) θ–2θ XRD patterns measured with a title angle = 54.7°.

perpendicular to the (111) plane,[8,22] the polar MOKE is expected to reach its maximum when the light propagates parallel to the [111] axis.

The (111)-oriented Mn_3Ir films with a thickness of 20 nm were epitaxially grown on MgO (111) substrates using magnetron sputtering under a base pressure of 1.5×10^{-5} Pa. The sputtering target was an arc-melted Mn75%-Ir alloy. Substrate temperatures during the Mn_3Ir growth were T_s = 800 and 600 °C for samples I and II, respectively. The Mn_3Ir growth was followed by the deposition of a 5-nm-thick SiO_2 overlayer. Mn_3Ir films prepared under the same deposition conditions exhibit a prominent anomalous Hall effect.[15–17]

Figures 1(c) and 1(d) show x-ray diffraction (XRD) data using a Cu-$K\alpha$ source for samples I and II. Figure 1(c) shows non-tilted (ψ = 0°), standard θ–2θ XRD data, which indicate that the primary diffraction peaks of Mn_3Ir (111) for both samples are epitaxial Mn_3Ir (111) layers. The spacing of Mn_3Ir (111) was d_{111} = 0.218 nm for both samples, coinciding well with that of a Mn_3Ir bulk crystal, d_{111} = 0.2181 nm.[27] In view of the large lattice mismatch ($\Delta a/a_{MgO} \approx 10\%$) between cubic MgO and cubic $L1_2$-Mn_3Ir, it is reasonable to assume that 20-nm-thick epilayers are fully relaxed in terms of heteroepitaxial growth. Figure 1(d) shows the asymmetric θ–2θ XRD data with a tilt angle of ψ = 54.7° for both samples. Note that the extent of $L1_2$ ordering can be estimated by comparing the diffraction intensity between (001), the $L1_2$-ordered-superlattice diffraction plane, and (002), the extinction-rule-allowed diffraction plane.[28] The (001) lattice spacings determined by the (002) diffraction were d_{100} = 0.380 and 0.381 nm for sample I (T_s = 800 °C) and sample II (T_s = 600 °C), respectively. The difference in d_{100} exceeded the resolution limit of the XRD measurements. Both samples exhibited a somewhat larger (001) lattice spacing than the literature value for bulk Mn_3Ir, a_{100} = 0.3778 nm.[27] Specifically, the deviation from the bulk (001) spacing is slightly larger for the low-T_s sample than for the high-T_s sample. The fact that d_{001} differs whereas d_{111} is the same between the two samples suggests plastic deformation of the epilayers, which lowers the crystal symmetry. Moreover, to determine the degree of cube-on-cube growth, we performed φ-XRD scan at ψ = 54.7° and obtained $2\theta = 2\theta_{002}$ for the Mn_3Ir films [Figs. S3(a) and S3(b)] and the MgO substrate [Fig. S3(c)]. The φ-XRD scans indicate the existence of crystal twinning in sample I and sample II. The twinning ratios are estimated to be 0.29 and 0.33 for sample I and sample II, respectively, from the integrated values of the diffraction peaks.

As mentioned in the previous paragraph, the appearance of the (001) diffraction peak indicates the existence of $L1_2$ ordering.[29] The order parameter S can be estimated from the integrated intensities of the (001) peak, I_{001}, and the fundamental (002) peak, I_{002}, using the following equation:[29,28]

$$S = \sqrt{\frac{I_{001}(f_{Ir} + 3f_{Mn})^2 LP(\theta_{002})A(\theta_{002})}{I_{002}(f_{Ir} - f_{Mn})^2 LP(\theta_{001})A(\theta_{001})}}. \quad (1)$$

Here, we considered the Lorentz-polarization factor, $LP(\theta) = (1 + \cos^2 2\theta)/\sin^2\theta \cos\theta$, and absorption factor, $A(\theta) = (1 - e^{-\frac{2\mu t}{\sin\theta}})/2\mu$, with the absorption coefficient μ = 0.251 μm^{-1} at the diffraction-peak positions, $\theta = \theta_{001}$ and $\theta = \theta_{002}$. The ratio of the structure factors was $(f_{Ir} - f_{Mn})^2/(f_{Ir} + 3f_{Mn})^2$ = 0.1170. The S values calculated on the basis of these physical quantities are 0.47 and 0.28 for samples I and II, respectively. It is worth noting that the difference in the growth temperature of 200 °C affects both crystal deformation and $L1_2$ ordering.

To visualize the domain structure at room temperature, we built a scanning magneto-optical setup equipped with He–Ne laser (wavelength, λ = 632.8 nm), as schematically shown in Fig. S1. Horizontally(x) polarized light was incident perpendicular to the surface of a Mn_3Ir film mounted on a stage whose lateral motion was controlled by two stepping motors. The light beam was focused on the surface with a diameter of ~2 μm using a long-working-distance objective lens with a magnification of 20. We used a polarization-modulation technique using a photo-elastic modulator.[30] In our configuration, the horizontally(x) polarized component of the reflected light is modulated using a photoelastic modulator at a frequency of 42 kHz. After the linear polarization direction was rotated by π/4 using a λ/2 wave plate, the horizontally(x) polarized and perpendicularly(y) polarized components were separated by a Wollaston prism and measured using a balanced photo detector. The fundamental-frequency (42 kHz) and double-frequency (84 kHz) AC output voltages were measured using lock-in amplifiers. The DC voltage was simultaneously measured using a multimeter. We determined the polar-magneto-optical Kerr rotation φ_K and ellipticity η_K angles by calculating the ratios of the AC voltages to the DC voltage,

considering reflections at interfaces. See the supplementary material for more details on the measurement setup and analysis method.

Figures 2(a) and 2(b) show the φ_K and η_K spatial images of sample I, respectively. Both φ_K and η_K spatial images have a similar maze pattern with opposite signs. The domain width is several micrometers, which is larger than that of polycrystalline Mn_3Ir films, <2 μm.[17] The wide domain-wall widths of a few micrometers are attributed to the spot size of a laser beam; the realistic domain-wall width is supposed to be hundreds of nanometers.[31] Subsequently, we show the φ_K and η_K spatial images of sample II in Figs. 2(c) and 2(d), respectively. The mixture of maze and stripe patterns is observed for sample II, whereas the φ_K and η_K spatial images indicate opposite polarities. The domain size was approximately half that of sample I. The difference in domain size may be caused by the in-plane lattice strain. Similar to the closure magnetic domains of ferromagnets with no net magnetic-dipole energy,[32] in antiferromagnetic Mn_3Ir films, magnetostriction may compete with the domain wall energy to determine the magnetic width.

We next evaluated the values of φ_K and η_K of the Mn_3Ir films. Because of the difficulty in making a uniformly magnetized state, we excluded intermediate values less than 25 (2) and 9 (5) mdeg for the $|\varphi_K|$ and $|\eta_K|$ spatial images of sample I and sample II, respectively, assuming that the intermediate values result from magnetic domain walls, where spins gradually rotate.[31] Since completely removing regions associated with domain walls is difficult, our analysis process would result in underestimating the values of $|\varphi_K|$ and $|\eta_K|$. By averaging the values of the remaining pixels, we consequently obtained $|\varphi_K| = 41.6 \pm 0.3$ (4.5 ± 0.1) mdeg and $|\eta_K| = 15.3 \pm 0.1$ (9.1 ± 0.1) mdeg for sample I (sample II). Notably, the $|\varphi_K|$ value of sample I is enhanced several times higher than those of Mn_3Sn[7] ($|\varphi_K|$ ~20 mdeg) and Mn_3Ge[19] ($|\varphi_K|$ ~8.2 mdeg) single crystals, despite the imperfect crystallinity of our sample. This is consistent with our original expectation that a large MOKE emerges in $L1_2$-Mn_3Ir for a large SOC in the Ir ions.

To determine whether the observed pattern is truly magnetic, we studied the response of the magnetic domain pattern to an external magnetic field. In the following experiment, we applied a magnetic field of ±90 kOe normal to the Mn_3Ir film surface by using a superconducting magnet at 300 K and then brought them back to the MOKE setup. The field strength of ±90 kOe would be sufficiently large to obtain a minor hysteresis response, considering previous electrical transport measurements of similar $L1_2$-Mn_3Ir films.[15–17] To scan the same area before and after magnetic field application, we made cross-shaped scratches close to the scanning area as a marker. Slight changes are noticeable in Figs. 3(a)–3(d), which show φ_K special images obtained after the application of external fields of ±90 kOe for sample I and sample II. The observed changes are attributed to the small remanence magnetization and the minor response within the employed range of magnetic field.[16] In detail, for sample I, applying a magnetic field of +90 kOe increases the red portions of the φ_K spatial image [Fig. 3(a)] in comparison with those obtained after applying −90 kOe [Fig. 3(b)]. In contrast, for sample II, the red portion of the φ_K spatial image decreased upon applying a magnetic field of +90 kOe [Fig. 3(c)] relative to the spatial image shown in Fig. 3(d). Hence, because A and B spin configurations have positive and negative tiny net magnetization, respectively,[8] the A phase with a positive net magnetization should have positive (negative) φ_K for sample I (sample II). An artificial compression of the order of 0.1% imposed on a Mn_3Sn single crystal

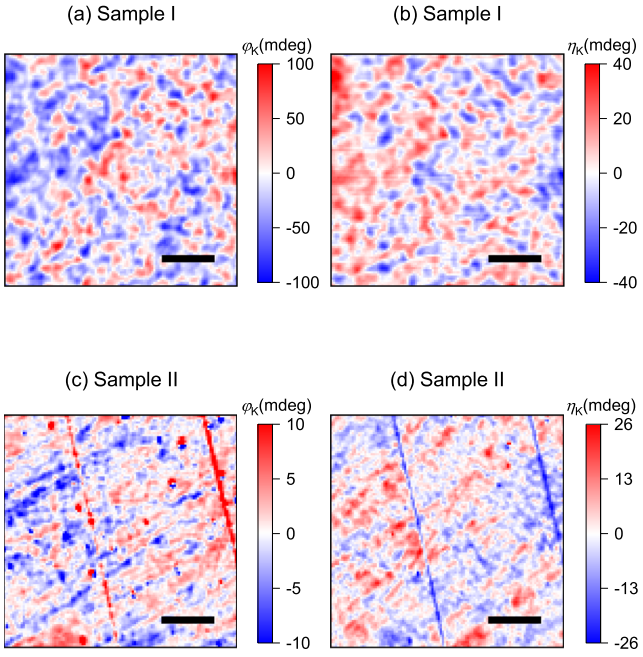

FIG. 2. (a)–(d) Magnetic domain patterns visualized by Kerr rotation (φ_K) and ellipticity (η_K) angles of samples I and II. The scale bars correspond to 50 μm.

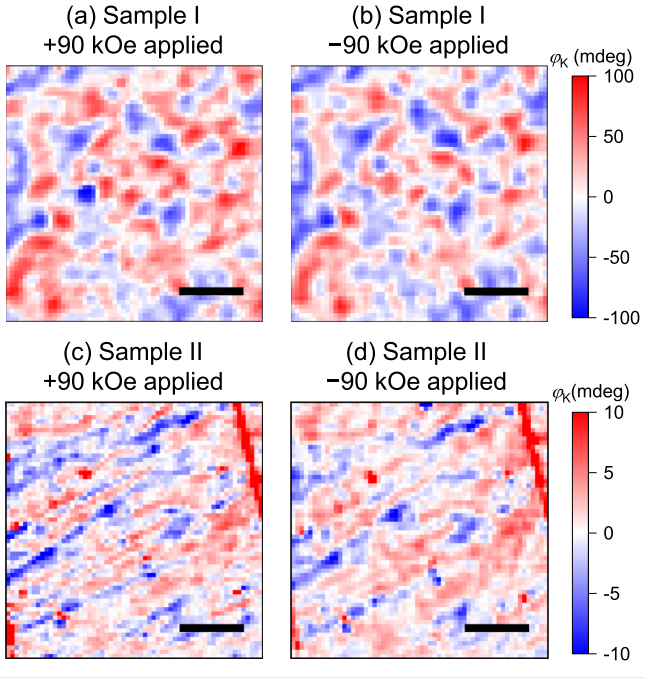

FIG. 3. (a)–(d) Transformation of the magnetic domain patterns of samples I and II after applying a magnetic field of +90 or −90 kOe. The scale bars correspond to 30 μm.

TABLE I. The (magneto-)optical properties of the Mn_3Ir films.

		Sample I	Sample II
T_s	°C	800	600
$n - i\kappa$		2.75–*i*3.65	2.01–*i*4.64
$\sigma'_{xx} - i\sigma''_{xx}$	$10^3\ \Omega^{-1}\ cm^{-1}$	5.31–*i*1.78	4.90–*i*4.88
$\varphi_K - i\eta_K$	mdeg	41.6 ± 0.5 + *i*(15.3 ± 0.1)	−4.5 ± 0.1–*i*(9.1 ± 0.01)
$\sigma'_{xy} - i\sigma''_{xy}$	$\Omega^{-1}\ cm^{-1}$	−17.5 ± 0.1 + *i*(15.5 ± 0.1)	5.9 ± 0.1–*i*(6.7 ± 0.1)

substantially changes the amplitude of the anomalous Hall effect.[33] For the case of the Mn_3Sn single crystal, the sign inversion by compression is supposed to be due to switching the parallel alignment of the cluster octupole and the net magnetic moments to an antiparallel alignment. In contrast, since the anomalous Hall effect of Mn_3Ir films is not inverted according to the growth temperatures,[16] we infer that the variation and sign inversion of the MOKE between sample I and sample II grown at two different T_s are attributed to changes in the electronic structures by the lattice deformation along the [001] direction rather than switching the alignment of the cluster octupole and the net magnetic moments. With increasing growth temperature, the lattice constant tends to relax into the bulk value.[34] By further increasing the growth temperature, the amplitudes of the magneto-optical effect may approach the bulk values, for instance, those predicted by an *ab initio* calculation.[9]

Using the values of φ_K and η_K, we finally evaluated the off-diagonal components of the optical conductivity tensor. The off-diagonal component of the complex optical conductivity, $\sigma_{xy} = \sigma'_{xy} - i\sigma''_{xy}$, is estimated using the following relation:

$$\varphi_K - i\eta_K = \frac{-\sigma_{xy}}{\sigma_{xx}\sqrt{1 - i(4\pi/\omega)\sigma_{xx}}}, \tag{2}$$

where ε_0, ω, and σ_{xx} denote the permittivity of vacuum, angular frequency of light at λ = 632.8 nm, and diagonal component of the complex optical conductivity, respectively, $\sigma_{xx} = \sigma'_{xx} - i\sigma''_{xx}$. We measured the refractive indices of the Mn_3Ir films, $n - i\kappa$, using a standard ellipsometer at λ = 632.8 nm. The values of the refractive index were used to estimate the diagonal component of the complex optical conductivity, based on the following relation: $1 - i(4\pi/\omega)\sigma_{xx} = (n - i\kappa)^2$. Table I lists the calculated (magneto-)optical properties. The values of σ'_{xy} of sample I are observed to be approximately half of the reported anomalous Hall conductivities,[16] $\sigma'_{xy} = -32\ \Omega^{-1}\ cm^{-1}$. To the best of our knowledge, this is the first study to report the off-diagonal optical conductivity of a Kagome antiferromagnet by characterizing both the magneto-optical Kerr rotation and ellipticity angles in the visible spectral range.

In summary, we measured the polar MOKE of (111)-oriented $L1_2$-Mn_3Ir films, which comprise a noncollinear spin configuration and large spin orbit coupling. From the visualized magnetic domains, we evaluated the magneto-optical Kerr rotation and ellipticity angles. The magneto-optical Kerr rotation angle of the (111)-oriented $L1_2$-Mn_3Ir films grown at 800 °C is several times larger than those observed in single-crystalline Mn_3Sn and Mn_3Ge systems. We also observed polarity inversion of the MOKE between two samples grown at different substrate temperatures and discussed that this is owing to a slight change in the in-plane lattice constant. Our results indicate the critical impact of the crystal structure, including the order parameter and slight lattice distortion, on the magneto-optical Kerr effect in Kagome-type antiferromagnets.

The supplementary material includes a more detailed description of the magneto-optical setup and x-ray diffraction φ scans.

We thank Professor S. Nakagawa, Mr. H. Kumagai, Dr. H. Iida, and Dr. Y. Suzuki for technical guidance with the XRD measurements and Ms. M. Takumi for carefully checking the Jones calculations. This study was partially supported by JSPS KAKENHI (Grant Nos. 19H01828, 19H05618, 19K21854, 20H05665, 21H01032, 21H04562, 22K14588, 22H01154, and 24K00938), JST PRESTO (Grant No. JPMJPR20B9), Frontier Photonic Sciences Project (Grant Nos. 01212307, 01212405, 01212002, and 01213004), OML Project (Grant No. OML012301) from NINS and MEXT X-NICS (Grant No. JPJ011438), and the Collaborative Research Program of the Institute for Chemical Research, Kyoto University.

AUTHOR DECLARATIONS

Conflict of Interest

The authors have no conflicts to disclose.

Author Contributions

K.T.Y. and K.Y. equally contributed to this work.

Kihiro T. Yamada: Conceptualization (lead); Data curation (lead); Formal analysis (lead); Funding acquisition (equal); Investigation (lead); Methodology (equal); Project administration (equal); Software (equal); Supervision (equal); Visualization (lead); Writing – original draft (lead); Writing – review & editing (lead). **Kotarou Yamaguchi**: Formal analysis (equal); Investigation (equal); Methodology (lead); Software (lead); Visualization (supporting); Writing – original draft (equal); Writing – review & editing (equal). **Yuta Kobayashi**: Resources (lead); Writing – original draft (supporting); Writing – review & editing (supporting). **Yota Takamura**: Investigation (supporting); Methodology (supporting); Writing – original draft (supporting); Writing – review & editing (supporting). **Hiro Munekata**: Methodology (supporting); Writing – original draft (supporting); Writing – review & editing (supporting). **Teruo Ono**: Funding acquisition (supporting); Resources (supporting); Writing – original draft (supporting); Writing – review & editing

(supporting). **Takahiro Moriyama**: Funding acquisition (supporting); Resources (equal); Writing – original draft (supporting); Writing – review & editing (supporting). **Takuya Satoh**: Funding acquisition (lead); Project administration (lead); Supervision (lead); Writing – original draft (equal); Writing – review & editing (equal).

DATA AVAILABILITY

The data that support the findings of this study are available from the corresponding author upon reasonable request.

REFERENCES

[1] H. Ebert, Rep. Prog. Phys. **12**, 1665–1735 (1996).
[2] H. J. Williams, F. G. Foster, and E. A. Wood, Phys. Rev. **82**, 119 (1951).
[3] J. McCord, J. Phys. D: Appl. Phys. **48**, 333001 (2015).
[4] Y. K. Kato, R. C. Myers, A. C. Gossard, and D. D. Awschalom, Science **306**, 1910–1913 (2004).
[5] B. Huang, G. Clark, E. Navarro-Moratalla, D. R. Klein, R. Cheng, K. L. Seyler, D. Zhong, E. Schmidgall, M. A. McGuire, D. H. Cobden, W. Yao, D. Xiao, P. Jarillo-Herrero, and X. Xu, Nature **546**, 270–273 (2017).
[6] C. Gong, L. Li, Z. Li, H. Ji, A. Stern, Y. Xia, T. Cao, W. Bao, C. Wang, Y. Wang, Z. Q. Qiu, R. J. Cava, S. G. Louie, J. Xia, and X. Zhang, Nature **546**, 265–269 (2017).
[7] T. Higo, H. Man, D. B. Gopman, L. Wu, T. Koretsune, O. M. J. van 't Erve, Y. P. Kabanov, D. Rees, Y. Li, M. Suzuki, S. Patankar, M. Ikhlas, C. L. Chien, R. Arita, R. D. Shull, J. Orenstein, and S. Nakatsuji, Nat. Photonics **12**, 73–78 (2018).
[8] H. Chen, Q. Niu, and A. H. MacDonald, Phys. Rev. Lett. **112**, 017205 (2014).
[9] W. Feng, G.-Y. Guo, J. Zhou, Y. Yao, and Q. Niu, Phys. Rev. B **92**, 144426 (2015).
[10] M.-T. Suzuki, T. Koretsune, M. Ochi, and R. Arita, Phys. Rev. B **95**, 094406 (2017).
[11] S. Nakatsuji, N. Kiyohara, and T. Higo, Nature **527**, 212–215 (2015).
[12] A. K. Nayak, J. E. Fischer, Y. Sun, B. Yan, J. Karel, A. C. Komarek, C. Shekhar, N. Kumar, W. Schnelle, J. Kübler, C. Felser, and S. S. P. Parkin, Sci. Adv. **2**, e1501870 (2016).
[13] N. Kiyohara, T. Tomita, and S. Nakatsuji, Phys. Rev. Appl. **5**, 064009 (2016).
[14] Z. Q. Liu, H. Chen, J. M. Wang, J. H. Liu, K. Wang, Z. X. Feng, H. Yan, X. R. Wang, C. B. Jiang, J. M. D. Coey, and A. H. MacDonald, Nat. Electron. **1**, 172–177 (2018).
[15] H. Iwaki, M. Kimata, T. Ikebuchi, Y. Kobayashi, K. Oda, Y. Shiota, T. Ono, and T. Moriyama, Appl. Phys. Lett. **116**, 022408 (2020).
[16] Y. Kobayashi, M. Kimata, D. Kan, T. Ikebuchi, Y. Shiota, H. Kohno, Y. Shimakawa, T. Ono, and T. Moriyama, Jpn. J. Appl. Phys. **61**, 070912 (2022).
[17] Y. Kobayashi, T. Ikebuchi, Y. Shiota, T. Ono, T. Moriyama, and J. Magn, J. Magn. Soc. Jpn. **45**, 75–78 (2021).
[18] A. L. Balk, N. H. Sung, S. M. Thomas, P. F. S. Rosa, R. D. McDonald, J. D. Thompson, E. D. Bauer, F. Ronning, and S. A. Crooker, Appl. Phys. Lett. **114**, 032401 (2019).
[19] M. Wu, H. Isshiki, T. Chen, T. Higo, S. Nakatsuji, and Y. Otani, Appl. Phys. Lett. **116**, 132408 (2020).
[20] Y. Otani and T. Higo, Appl. Phys. Lett. **118**, 040501 (2021).
[21] T. Uchimura, J.-Y. Yoon, Y. Sato, Y. Takeuchi, S. Kanai, R. Takechi, K. Kishi, Y. Yamane, S. Dutta Gupta, J. Ieda, H. Ohno, and S. Fukami, Appl. Phys. Lett. **120**, 172405 (2022).
[22] Y. Zhang, Y. Sun, H. Yang, J. Železný, S. P. P. Parkin, C. Felser, and B. Yan, Phys. Rev. B **95**, 075128 (2017).
[23] Y. Zhang, J. Železný, Y. Sun, J. van den Brink, and B. Yan, "Spin Hall effect emerging from a noncollinear magnetic lattice without spin–orbit coupling," New J. Phys. **20**, 073028 (2018).
[24] H. Chen, T.-C. Wang, D. Xiao, G.-Y. Guo, Q. Niu, and A. H. MacDonald, Phys. Rev. B **101**, 104418 (2020).
[25] Y. Yanase and H. Harima, Kotai Butsuri **46**(543), 229–239 (2001).
[26] I. Tomeno, N. Fuke, H. Iwasaki, M. Sahashi, and Y. Tsunoda, J. Appl. Phys. **86**, 3853–3856 (1999).
[27] B. Balke, S. Wurmehl, G. H. Fecher, C. Felser, and J. Kübler, Sci. Technol. Adv. Mater. **9**, 014102 (2008).
[28] B. D. Cullity and S. R. Stock, *Elements of X-Ray Diffraction*, 3rd ed. (Prentice Hall, 2001).
[29] A. A. Jara, I. Barsukov, B. Youngblood, Y.-J. Chen, J. Read, H. Chen, P. Braganca, and I. N. Krivorotov, IEEE Magn. Lett. **7**, 3104805 (2016).
[30] K. Sato and T. Ishibashi, Front. Phys. **10**, 946515 (2022).
[31] S. Sugimoto, Y. Nakatani, Y. Yamane, M. Ikhlas, K. Kondou, M. Kimata, T. Tomita, S. Nakatsuji, and Y. C. Otani, Commun. Phys. **3**, 111 (2020).
[32] H. J. Williams, R. M. Bozorth, and W. Shockley, Phys. Rev. **75**, 155 (1949).
[33] M. Ikhlas, S. Dasgupta, F. Theuss, T. Higo, S. Kittaka, B. J. Ramshaw, O. Tchernyshyov, C. W. Hicks, and S. Nakatsuji, Nat. Phys. **18**, 1086–1093 (2022).
[34] J. M. Taylor, E. Lesne, A. Markou, F. K. Dejene, B. Ernst, A. Kalache, K. G. Rana, N. Kumar, P. Werner, C. Felser, and S. S. P. Parkin, Phys. Rev. Mater. **3**, 074409 (2019).